Superballistic boundary conductance and hydrodynamic transport in microstructures

O. E. Raichev
Institute of Semiconductor Physics, NAS of Ukraine, Prospekt Nauki 41, 03028 Kyiv, Ukraine

(Received 3 February 2022; revised 27 July 2022; accepted 28 July 2022; published 8 August 2022)

It is shown that the ideal boundary between a perfectly conducting electrode and electron liquid state acts as a contact whose conductance per unit area is higher than the fundamental Sharvin conductance by a numerical coefficient 2α, where α is slightly smaller than unity and depends on the dimensionality of the system. If the boundary has a finite curvature, an additional correction to the boundary conductance appears, which is parametrically small as a product of the curvature by the electron-electron mean free path length. The relation of the normal current density to the voltage between the electrode and electron liquid represents itself a hydrodynamic boundary condition for current-penetrable boundary. Calculations of the conductance and potential distribution in microstructures by means of numerical solution of the Boltzmann equation show that the concept of boundary conductance works very good when the hydrodynamic transport regime is reached. The superballistic transport, when the device conductance is higher than the Sharvin conductance, can be realized in Corbino disk devices not only in the hydrodynamic regime, although requires that the electron-electron scattering rate must be higher than the momentum-relaxing scattering rate. The theoretical results for Corbino disks are consistent with recent experimental findings.

DOI: 10.1103/PhysRevB.106.085302

I. INTRODUCTION

In the last years, there is a large progress in the studies of the hydrodynamic transport regime for electron gas in solid state conductors, when electron motion resembles the dynamics of viscous fluids[1–10]. This regime takes place under condition that the mean free path length with respect to momentum-conserving electron-electron (ee) scattering l_e is much smaller than the other characteristic lengths of the system, namely the transport mean free path length l_{tr} describing momentum-relaxing (electron-impurity and electron-phonon) scattering and the lengths relevant to the conductor geometry. Since l_e rapidly decreases with temperature, $l_e \propto T^{-2}$, the hydrodynamic regime can be reached by increasing electron temperature in high-mobility two-dimensional (2D) electron gas, where l_{tr} is minimized. Some important manifestations of the hydrodynamic behavior include unusual temperature dependence of electrical resistance [11–13], viscous magnetoresistance and Hall viscosity effects [14–17], and nonlocal transport phenomena caused by collective hydrodynamic motion [18–23]. Substantial modifications of the current and potential profiles, with corresponding influence on the resistance, occur in mesoscopic conductors under a transition from the ballistic to the hydrodynamic transport regime [24–30]. It has been also found [31–35] that in the hydrodynamic regime the conductance of microcontacts can be higher than the conductance in the ballistic transport regime. This property, often called as superballistic transport, has been experimentally verified in narrow 2D constrictions (point contacts) with widths of the order of one micron, based on graphene [32] and GaAs heterostructures [33]. Recently, the signatures of possible superballistic behavior have been also detected in high-quality graphene Corbino disks of several micron size [35].

The fundamental upper bound of the ballistic conductance is given by the Sharvin conductance equal to the conductance quantum $e^2/2\pi\hbar$ multiplied by the number of quantum channels able to carry the electrons through the contact (open channels). In the case of classical transport, this number is large and proportional to the area of the contact. The ideal ballistic Sharvin contact can be viewed as a hole in a thin nonpenetrable wall separating two regions where electron gas stays in quasiequilibrium characterized by different electrochemical potentials U_1 and U_0 [36]. A similar setup is realized in a point contact representing a smooth constriction between two regions, so the hole is identified with the narrowest place of this constriction. The Sharvin contact can be also created by placing a thin conducting layer, where electrons move ballistically, between two perfectly conducting electrodes, also called below as leads, as shown in Fig. 1(a). It is assumed that the boundaries between the leads and the layer are ideal so that electrons pass them without backscattering. All such systems are characterized by the Sharvin conductance $G_S = I/U$, where I is the total current passing through the contact and $U = U_1 - U_0$ is the applied voltage. For the systems with uniform current-penetrable boundaries (Fig. 1), it is also convenient to introduce the normal current density j_n and the Sharvin conductance per unit square of the contact area (for 2D case, per unit length), $\mathcal{G}_S = j_n/U$. This conductance depends on the electron energy spectrum, electron density n, and temperature T.

The theoretical explanation of the superballistic transport in constrictions [31,32,34] is based on the fact that in the hydrodynamic regime the motion of electrons is collective

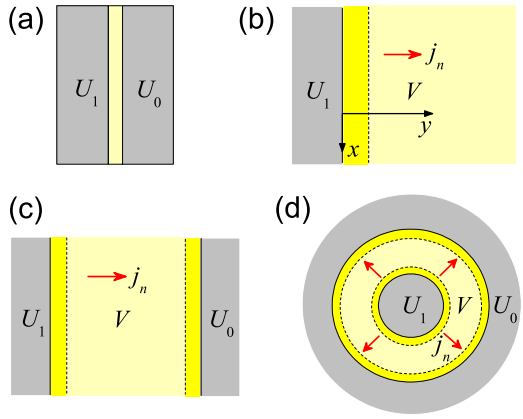

FIG. 1. (a) A thin conducting layer, where electrons move ballistically, is sandwiched between two perfectly conducting electrodes with fixed electrochemical potentials, forming the Sharvin contact. (b) The contact between the electrode and the electron liquid staying at electrochemical potential V spreads over the Knudsen layer (bright yellow), where the potential changes rapidly. The normal current flowing through the contact is indicated by the red arrow. [(c),(d)] Devices of flat geometry and Corbino geometry with the contacts described above.

and differs from the individual electron motion in the ballistic (Knudsen) regime. The Landauer interpretation of the contact conductance in the form given above is no longer valid for such hydrodynamic flow, though the concept of quantum channels still remains [34]. The number of these channels varies along the constriction, dropping down to the number of open channels in the narrowest place. In the process of motion, electron-electron scattering transfers carriers from the terminated channels, in which the ballistic electrons would scatter back, to the open channels, thereby helping them to pass the contact. To summarize, although the number of open channels remains the same, the electrons in the hydrodynamic regime use these channels more often than in the ballistic regime, so the conductance increases. The theory [31,34] predicts that the conductance increases over the Sharvin one by a factor proportional to the constriction length divided by l_e. Thus, it was concluded [34] that, in terms of parameters, the conductance can be made arbitrary large.

The superballistic transport in the systems with sharp contact boundaries (Fig. 1) requires a different explanation. The main goal of this paper is to describe the transport mechanism in such systems and to find a specific conductance associated with the presence of the boundary and below referred to as the boundary conductance. The results are also applied to transport in microstructures. The consideration is based on the concept that the interface between the electrode and the electron liquid can be viewed as a quasiballistic Sharvin-like contact. Indeed, the hydrodynamic state away from the boundary is characterized by its own electrochemical potential V and current density $\mathbf{j}$ governed by the continuity equation and the Navier-Stokes equation. The spatial variation of these quantities occurs on a much larger scale than the width of the Knudsen layer separating the hydrodynamic state from the lead, Fig. 1(b). The linear relation between the normal inward current density and the potential drop ΔU between the lead and the electron liquid is written as

$$j_n = \mathcal{G}\Delta U. \tag{1}$$

The conductance per unit area of the boundary $\mathcal{G}$ is considered in Sec. II. It is shown that the upper bound of $\mathcal{G}$ is equal to $2\mathcal{G}_S$, while the numerical calculations based on the Boltzmann equation formalism show that the ratio $\mathcal{G}/\mathcal{G}_S$ is slightly smaller than 2. The result depends on dimensionality as well as on the model of electron-electron collision integral. Thus, the contact between the lead and the electron system in the hydrodynamic state is superballistic. However, in contrast to the constriction described above, such a contact cannot provide arbitrary large conductance. Section III contains calculations of the conductance and potential profile for the devices of highly symmetric geometries shown in Figs. 1(c) and 1(d) for different transport regimes. In particular, it is shown that the Corbino disk devices can demonstrate the superballistic conductance caused by strong electron-electron interaction, and not only in the hydrodynamic regime. Connection of the presented theory to the recent experiment [35] is also discussed. Concluding remarks are given in Sec. IV.

II. BOUNDARY CONDUCTANCE

Since the interface between the perfectly conducting electrode and the hydrodynamic electron state spreads over the Knudsen layer width, which is much smaller than any other hydrodynamic length parameter of the system, it is sufficient to consider a homogeneous flat contact boundary and a constant normal current density j_n, as shown in Fig. 1(b). The current density is constant according to the continuity equation $\nabla \cdot \mathbf{j} = 0$. A tangential current density can also be present in the system, but it is not relevant for calculations of the boundary conductance because the tangential current does not affect the normal current and potential distribution on the scale of the Knudsen layer width estimated as l_e. This statement remains true even in the presence of a magnetic field parallel to the boundary if this field is sufficiently weak so the cyclotron radius is much larger than l_e.

The Knudsen layer exists because the distribution of electron momenta at the boundary is affected by injection of the electrons from the lead and, therefore, is different from the one in the hydrodynamic state. Thus, some space is needed to accommodate this distribution to the hydrodynamic form, which is achieved owing to electron-electron interaction. Description of the transport within the Knudsen layer requires solution of the Boltzmann kinetic equation for the distribution function of electrons in the system, $f_{\mathbf{p}}(\mathbf{r})$, where $\mathbf{p}$ is the electron momentum and $\mathbf{r}$ is the coordinate. The energy spectrum of electrons, $\varepsilon = \varepsilon_{\mathbf{p}}$, is assumed to be isotropic, although the results presented in the paper are applicable for arbitrary electronic dispersion ε_p. In the linear transport regime, it is convenient to present the distribution function as

$$f_{\mathbf{p}}(\mathbf{r}) = f_\varepsilon + \delta f_{\mathbf{p}}(\mathbf{r}) = f_\varepsilon - [g_{\mathbf{p}}(\mathbf{r}) - e\Phi(\mathbf{r})]\partial_\varepsilon f, \tag{2}$$

where f_ε is the equilibrium Fermi-Dirac distribution, $\partial_\varepsilon f \equiv \partial f_\varepsilon/\partial\varepsilon$ and $\Phi(\mathbf{r})$ is the electrostatic potential that is equal to zero in equilibrium. The function $g_{\mathbf{p}}(\mathbf{r})$ describes the

nonequilibrium response. In particular, the current density is

$$\mathbf{j}(\mathbf{r}) = e\int d\varepsilon D_\varepsilon \overline{\mathbf{v}_\mathbf{p} g_\mathbf{p}(\mathbf{r})}(-\partial_\varepsilon f), \tag{3}$$

where D_ε is the density of states and $\mathbf{v}_\mathbf{p}$ is the group velocity. The overline symbol denotes averaging over the angles of momentum. The nonequilibrium part of electrochemical potential $V(\mathbf{r})$ is determined by the isotropic part of $g_\mathbf{p}$, denoted below as $\overline{g}$,

$$eV(\mathbf{r}) = \overline{\langle g_\mathbf{p}(\mathbf{r})\rangle} = \langle \overline{g}(\mathbf{r})\rangle. \tag{4}$$

Here and below, the average of an arbitrary function F over energy is defined as

$$\langle F\rangle \equiv \int d\varepsilon D_\varepsilon v_\varepsilon p_\varepsilon(-\partial_\varepsilon f)F_\varepsilon/nd,$$

in view of the identity $nd = \int d\varepsilon D_\varepsilon v_\varepsilon p_\varepsilon(-\partial_\varepsilon f)$, where v and p are the absolute values of the group velocity and momentum, and d is the dimensionality of the system. Equation (4) is consistent with the definition $V(\mathbf{r}) = \delta\mu(\mathbf{r})/e + \Phi(\mathbf{r})$, where $\delta\mu(\mathbf{r})$ is the nonequilibrium part of the chemical potential. In the hydrodynamic regime, when $\overline{\delta f_\mathbf{p}(\mathbf{r})} = -\delta\mu(\mathbf{r})\partial_\varepsilon f$, $\overline{g}(\mathbf{r})$ is energy independent and $\overline{g}(\mathbf{r}) = eV(\mathbf{r})$. For degenerate electron gas, the average over energy fixes the energy variable at the Fermi energy, $\varepsilon = \varepsilon_F$, so $eV(\mathbf{r})$ is equal to $\overline{g}(\mathbf{r})$ taken at the Fermi energy. It is important to emphasize that, in the static linear response regime considered in this paper, both the electrochemical potential and the current density are determined by $g_\mathbf{p}(\mathbf{r})$ found from the kinetic equation [see Eq. (11) below] that does not contain modified electron density and electrostatic potential Φ.

The function $g_\mathbf{p}(\mathbf{r})$ can be expanded in series of angular harmonics as

$$g_\mathbf{p} = \overline{g} + g_\alpha c_\alpha + Q_{\alpha\beta}(c_\alpha c_\beta - \delta_{\alpha\beta}/d) + \ldots, \tag{5}$$

where α and β are the Cartesian coordinate indices (the repeated indices, by convention, imply summation over them), and $\mathbf{c} = \mathbf{p}/p$ is the unit vector along the momentum. The vector $g_\alpha = d\overline{c_\alpha g_\mathbf{p}}$ and the tensor $Q_{\alpha\beta}$ depend on energy and coordinate. They are related to the drift velocity $u_\alpha = j_\alpha/en$ and to the momentum flux density tensor $\Pi_{\alpha\beta}$ as $u_\alpha = \langle g_\alpha/p\rangle$ and $\Pi_{\alpha\beta} = 2n\langle Q_{\alpha\beta}\rangle/(d+2)$. In the hydrodynamic regime, $g_\alpha = pu_\alpha$ and $Q_{\alpha\beta} = -p\upsilon\tau\frac{1}{2}(\nabla_\beta u_\alpha + \nabla_\alpha u_\beta)$, where τ is the relaxation time of the second angular harmonic of the distribution function, while the higher-order terms, denoted in Eq. (5) by the dots, should be neglected. The quantity $-\Pi_{\alpha\beta}$ describes the viscous stress tensor, $-\Pi_{\alpha\beta} = \eta(\nabla_\beta u_\alpha + \nabla_\alpha u_\beta)$, where $\eta = n\langle p\upsilon\tau\rangle/(d+2)$ is the dynamic viscosity.

Below, the axis normal to the boundary is chosen as Oy and the boundary is placed at $y = 0$, Fig. 1(b). The electrons moving to the right and to the left are described by the distribution functions $f^+_\mathbf{p} = f_\mathbf{p}|_{p_y>0}$ and $f^-_\mathbf{p} = f_\mathbf{p}|_{p_y<0}$, respectively, defined in the momentum half-space $p_y = p\sin\varphi > 0$. The functions $g^\pm_\mathbf{p}$ are introduced in a similar way. The boundary condition at the left side, $y = 0$, is written as

$$g^+_\mathbf{p}\big|_{y=0} = eU_1, \tag{6}$$

which corresponds to representation of $f^+_\mathbf{p}$ as an isotropic Fermi-Dirac distribution characterized by the quasi-Fermi level of the left electrode. This is a particular case of the in-flow boundary condition applied to current-penetrable boundaries in kinetic theory [37,38], and its form is justified by the basic assumptions that the electron density and conductivity in the electrode are much larger than those in the electron system at $y > 0$, and that the electrons pass the boundary without backscattering. The boundary condition at the right side, $y \gg l_e$, is derived from the known form of the distribution function, Eq. (5), taken in the hydrodynamic transport regime. Since the drift velocity is constant, the viscous stress at $y \gg l_e$ is zero, so that $g_\mathbf{p} = eV + p_y u_y$ and the boundary condition is

$$g^-_\mathbf{p}\big|_{y\gg l_e} = eV - (p/en)j_n\sin\varphi, \tag{7}$$

since $u_y = j_n/en$ and $p_y = \pm p\sin\varphi$ for $\varphi \in [0,\pi]$ in $g^\pm_\mathbf{p}$. The normal current density j_n is constant everywhere. According to Eq. (3), j_n at $y = 0$ is written as

$$j_n = e\int d\varepsilon D_\varepsilon v_\varepsilon(-\partial_\varepsilon f)\overline{[[g^+_\mathbf{p}(0) - g^-_\mathbf{p}(0)]\sin\varphi]}_+, \tag{8}$$

where $g_\mathbf{p}$ is expressed in terms of $g^\pm_\mathbf{p}$ and $\overline{[\ldots]}_+$ denotes angular averaging limited by the half space or half plane where $p_y > 0$. For three-dimensional (3D) systems, $\overline{[\ldots]}_+ \equiv \int_+ \frac{d\Omega}{4\pi}\ldots = (4\pi)^{-1}\int_0^{\pi/2} d\varphi\cos\varphi\int_0^{2\pi} d\chi\ldots$, where $d\Omega$ is the differential of the solid angle and χ is the angle of the tangential component of momentum in the boundary plane (xz). For 2D systems, $\overline{[\ldots]}_+ \equiv (2\pi)^{-1}\int_0^\pi d\varphi\ldots$.

To estimate the value of the boundary conductance and to show the physical mechanism responsible for its increase over the Sharvin conductance, an approximate calculation of the boundary conductance is carried out below, followed by the detailed calculation based on numerical solution of the Boltzmann equation. It is assumed that the scattering of the left-moving electrons in the Knudsen layer can be neglected in calculation of the normal current j_n. This means that $g^-_\mathbf{p}(0)$ in Eq. (8) is approximated by the form of $g^-_\mathbf{p}$ given by Eq. (7), so one obtains $g^+_\mathbf{p}(0) - g^-_\mathbf{p}(0) = e(U_1 - V) + (p/en)j_n\sin\varphi$. This assumption is justified by the subsequent numerical calculations demonstrating that the calculated boundary conductance appears to be very close to the approximate one. By noticing that the Sharvin conductance per unit area is

$$\mathcal{G}_S = e^2\int d\varepsilon D_\varepsilon v_\varepsilon(-\partial_\varepsilon f)\overline{[\sin\varphi]}_+, \tag{9}$$

one can find that the potential term in the expression for $g^+_\mathbf{p}(0) - g^-_\mathbf{p}(0)$ produces the Sharvin current density $\mathcal{G}_S\Delta U$, where $\Delta U = U_1 - V$, while the term proportional to j_n is equal to $j_n/2$. Thus, one obtains Eq. (1) with

$$\mathcal{G}/\mathcal{G}_S = 2, \tag{10}$$

so the boundary conductance $\mathcal{G}$ is twice larger than the Sharvin conductance. The derivation of Eq. (10) shows that the superballistic effect occurs because the boundary condition for the left-moving electrons includes the term proportional to the current density j_n. Without this term, one would obtain the usual Sharvin conductance $\mathcal{G} = \mathcal{G}_S$. Physically, the presence of the current modifies the distribution function in the half space $y > 0$, in contrast to the perfectly

conducting region at $y < 0$, where such a modification is negligibly small. This increases electron transmission, because the backward, proportional to $f_{\mathbf{p}}^{-}$, component of the current decreases, so the difference $g_{\mathbf{p}}^{+} - g_{\mathbf{p}}^{-}$ gains a positive contribution proportional to j_n.

The result of Eq. (10) is approximate because the scattering of the left-moving electrons in the Knudsen layer has been neglected. Thus, Eq. (10) gives the upper bound of the conductance $\mathcal{G}$ in Eq. (1). To obtain a more precise result, one should solve the kinetic equation with boundary conditions Eqs. (6) and (7). The kinetic equation in the linear transport regime is transformed to an equation for $g_{\mathbf{p}}$,

$$\mathbf{v}_{\mathbf{p}} \cdot \nabla g_{\mathbf{p}}(\mathbf{r}) = J_{\mathbf{p}}(\mathbf{r}), \tag{11}$$

where the linearized collision integral is represented as $(-\partial_\varepsilon f)J_{\mathbf{p}}(\mathbf{r})$. The electrostatic potential Φ does not appear explicitly in Eq. (11) because it is already included to the isotropic part of $g_{\mathbf{p}}(\mathbf{r})$ according to Eq. (2). The collision-integral term $J_{\mathbf{p}}$ is written as a sum of momentum-relaxing (MR) and momentum-conserving electron-electron parts, $J_{\mathbf{p}} = J_{\mathbf{p}}^{MR} + J_{\mathbf{p}}^{ee}$. To specify them, the elastic relaxation-time approximation is used,

$$J_{\mathbf{p}}^{MR} = -\frac{g_{\mathbf{p}} - \overline{g}}{\tau_{tr}}, \tag{12}$$

and

$$J_{\mathbf{p}}^{ee} = -\frac{g_{\mathbf{p}} - \overline{g} - g_\alpha c_\alpha}{\tau_e}, \tag{13}$$

where τ_{tr} is the transport time and τ_e is the electron-electron scattering time. The corresponding lengths are introduced as $l_{tr} = v\tau_{tr}$ and $l_e = v\tau_e$. The approximation implies elastic isotropic scattering, which is strictly correct only in the case of scattering of electrons by short-range impurity potential. The nonelasticity of electron-phonon scattering entering $J_{\mathbf{p}}^{MR}$ can be neglected if the electron temperature exceeds the Bloch-Grüneisen temperature. Also, the nonelasticity of both electron-phonon and electron-electron scattering can be neglected at low temperatures $T \ll \varepsilon_F$ provided that $g_{\mathbf{p}}$ is not varied considerably as a function of energy within the interval $\sim T$ around the Fermi level. The isotropic scattering approximation for the electron-electron collision integral, which leads to representation of $J_{\mathbf{p}}^{ee}$ in terms of a single relaxation time τ_e, is, strictly speaking, not a good one, so it should be considered as a convenient model rather than a justifiable approximation. Nevertheless, the single-time approximation Eq. (13) for the electron-electron collision integral is often used in theoretical calculations [8,9,12,15,27,29,30,35,39] since it satisfies the principal properties of particle and momentum conservation, $\overline{J_{\mathbf{p}}^{ee}} = 0$ and $\mathbf{p}\overline{J_{\mathbf{p}}^{ee}} = 0$, and provides the easiest way to solve the kinetic equation in spatially inhomogeneous case and to describe fundamental hydrodynamic effects. In particular, this approximation is physically reliable for description of the potential distribution within the Knudsen layer, which is considered in this paper. Application of a more elaborate expression for $J_{\mathbf{p}}^{ee}$, as shown below, does not lead to qualitative modifications of this distribution. The nonelasticity of electron-electron scattering is not expected to modify this distribution considerably even at $T \sim \varepsilon_F$, as far as the linear transport regime is assumed.

For the problem under the consideration [Fig. 1(b)], Eq. (11) takes the form

$$[\sin\varphi \nabla_y + l^{-1}] g_\varphi(y) = \overline{g}(y)/l + g_y \sin\varphi / l_e, \tag{14}$$

where $g_{\mathbf{p}}(\mathbf{r})$ is written as $g_\varphi(y)$, $g_y = d\overline{g_\varphi \sin\varphi}$ is y independent and proportional to the normal current density, and $l^{-1} \equiv l_e^{-1} + l_{tr}^{-1}$. Note that l_e, l, and g_φ depend on electron energy ε. The solution of Eq. (14) satisfying the boundary conditions Eqs. (6) and (7) can be written through the integrals of $\overline{g}(y)$. Below, the zero point of $V(y)$ is chosen at $y \gg l$. Since the hydrodynamic transport in the bulk is considered, the momentum-relaxing scattering in the Knudsen layer is neglected, $l_{tr}^{-1} = 0$ and $l = l_e$. Owing to the elastic approximation for the collision integral, the angular averaging of Eq. (14) leads to the continuity equation $\nabla_y g_y = 0$, which means that g_y is a constant. Thus, g_y is equal to its value at $y \gg l$ standing in the boundary condition Eq. (7), $g_y = pj_n/en$. With the use of identities $\overline{g}(y) = \overline{[(g_\varphi^+ + g_\varphi^-)]}_+$ and $g_y = d\overline{[(g_\varphi^+ - g_\varphi^-)\sin\varphi]}_+$, the problem is finally reduced to an integral equation for $\overline{g}(y)$,

$$\overline{g}(\tilde{y}) = e\Delta U S(\tilde{y}) + \int_0^\infty d\tilde{y}' K(\tilde{y}, \tilde{y}') \overline{g}(\tilde{y}'), \tag{15}$$

where $\tilde{y} = y/l$ and $\tilde{y}' = y'/l$ are the dimensionless coordinates,

$$S(\tilde{y}) = \zeta_0(\tilde{y}) - \zeta_1^2(\tilde{y})/\zeta_2(\tilde{y}), \tag{16}$$

$$K(\tilde{y}, \tilde{y}') = K_0(\tilde{y}, \tilde{y}') - \frac{\zeta_1(\tilde{y})}{\zeta_2(\tilde{y})} K_1(\tilde{y}, \tilde{y}'), \tag{17}$$

$$K_0(\tilde{y}, \tilde{y}') = \overline{[e^{-|\tilde{y}-\tilde{y}'|/\sin\varphi}/\sin\varphi]}_+,$$

$$K_1(\tilde{y}, \tilde{y}') = \mathrm{sgn}(\tilde{y} - \tilde{y}') \overline{[e^{-|\tilde{y}-\tilde{y}'|/\sin\varphi}]}_+, \tag{18}$$

and

$$\zeta_k(\tilde{y}) = \overline{[\sin^k\varphi e^{-\tilde{y}/\sin\varphi}]}_+. \tag{19}$$

Numerical solution of Eq. (15) allows one to find the function $\overline{g}(y)$ determining the potential distribution $V(y)$ and the current density j_n. The latter is given by Eq. (1), where, in contrast to Eq. (10), the conductance is smaller than $2\mathcal{G}_S$,

$$\frac{\mathcal{G}}{\mathcal{G}_S} = 2\alpha, \ \alpha = 1 - \frac{1}{\zeta_1(0)} \left\langle\!\!\left\langle \int_0^\infty d\tilde{y} \zeta_0(\tilde{y}) \frac{\overline{g}(\tilde{y})}{e\Delta U} \right\rangle\!\!\right\rangle. \tag{20}$$

In this equation, $\langle\langle \ldots \rangle\rangle \equiv \langle p^{-1} \ldots \rangle / \langle p^{-1} \rangle$ denotes the modified averaging over energy.

Since Eq. (14) at $l_e \ll l_{tr}$ contains only one length parameter $l = l_e$, the dimensionless ratio $\overline{g}(\tilde{y})/e\Delta U$ is a numerical function of the dimensionless coordinate $\tilde{y}$. This property is directly seen from Eq. (15). The function $\overline{g}(y)$ depends on energy because of the energy dependence of the relaxation length l. However, the integral standing in Eq. (20) is an energy-independent numerical constant that is not affected by the averaging over energy. Therefore, the coefficient α describing the lowering of the ratio $\mathcal{G}/\mathcal{G}_S$ below its upper bound of 2 is independent of temperature, electron energy spectrum, and electron-electron scattering rate. The calculation gives $\alpha \simeq 0.96$ and $\alpha \simeq 0.94$ for 2D and 3D cases, respectively. The reduction of the boundary conductance caused by electron

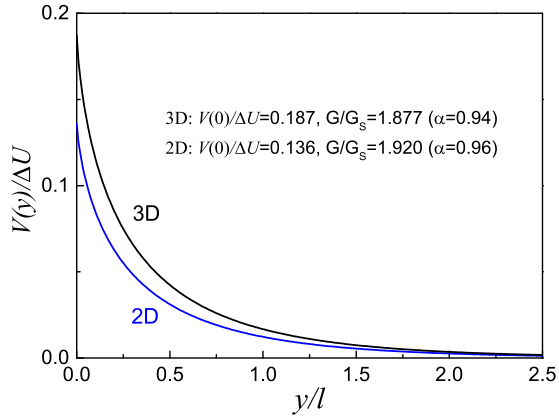

FIG. 2. Distribution of electrochemical potential in the Knudsen layer for the systems of different dimensionalities. The drop of the potential across the Knudsen layer and the boundary conductance are indicated.

collisions in the Knudsen layer appears to be relatively small, and the conductance remains superballistic.

For degenerate electron gas, when the electrochemical potential $V(y)$ is equal to $\overline{g}(y)/e$ at the Fermi energy ε_F, and l is fixed by its value at ε_F, the profile of $V(y)$ is shown in Fig. 2. The plots for 2D and 3D cases are similar and demonstrate that the main decrease of the potential occurs already at $y < l$. The total potential drop at the contact, ΔU, from the hydrodynamic point of view, can be described in terms of the pressure jump under injection of liquid between two different reservoirs. It includes a sharp jump of the electrochemical potential at the boundary and a smooth decrease within the Knudsen layer. The sharp jump is a consequence of chemical potential drop caused by the ballistic transfer of electrons between different media, whereas the smooth decrease appears because of the scattering of electrons within the Knudsen layer. The electrostatic potential $\Phi(y)$, which is related to the nonequilibrium density δn according to Poisson's equation, does not show a sharp jump, although it follows the electrochemical potential profile within the spatial scale of the screening length. The magnitude of the smooth part of the potential drop is relatively small. The normalized magnitude, $V(0)/\Delta U$, similar as α, depends only on the dimensionality.

The universality of the ratio $\mathcal{G}/\mathcal{G}_S$ described above is a consequence of the chosen model of the electron-electron collision integral, Eq. (13). A more careful consideration, even within the elastic approximation, suggests that this model is oversimplified because is describes the relaxation of all angular harmonics of electron distribution by a single time τ_e. In particular, it has been shown [40,41] and later emphasized [42,43] that, due to the kinematic constraints, the main contribution to the electron-electron collision integral at low temperatures comes from the head-on collisions that cause relaxation of the momentum-symmetric part of the electron distribution while leaving the antisymmetric part intact. As a result, the symmetric, $f^s_{\mathbf{p}} = (f_{\mathbf{p}} + f_{-\mathbf{p}})/2$, and antisymmetric, $f^a_{\mathbf{p}} = (f_{\mathbf{p}} - f_{-\mathbf{p}})/2$, parts of electron distribution are expected to relax with different times, τ_s and τ_a, respectively, and τ_a should be considerably larger than τ_s if T is much smaller than the Fermi energy ε_F. The simplest way to account this difference is to introduce the elastic two-time model [40],

$$J^{ee}_{\mathbf{p}} = -\frac{g^s_{\mathbf{p}} - \overline{g}}{\tau_s} - \frac{g^a_{\mathbf{p}} - g_\alpha c_\alpha}{\tau_a}, \tag{21}$$

that generalizes Eq. (13). This model can be applied as well to the problem of boundary conductance. Then, instead of Eq. (14), one has two equations

$$\begin{aligned} \sin\varphi \nabla_y g^a_\varphi(y) + g^s_\varphi(y)/l_s &= \overline{g}(y)/l_s, \\ \sin\varphi \nabla_y g^s_\varphi(y) + g^a_\varphi(y)/l_a &= g_y \sin\varphi/l_a, \end{aligned} \tag{22}$$

where $l_s = v\tau_s$, $l_a = v\tau_a$, and $l_{tr}^{-1} = 0$ is already implied. It is sufficient to define the functions $g^s_\varphi(y)$ and $g^a_\varphi(y)$ in the region $p_y > 0$, where $\sin\varphi$ is positive. Then, according to the symmetry of the problem, $g^\pm_\varphi(y) = g^s_\varphi(y) \pm g^a_\varphi(y)$. Solution of Eq. (22) with the boundary conditions Eqs. (6) and (7) leads to an integral equation of the same form as Eq. (15), where the dimensionless coordinates are now defined as $\tilde{y} = y/l_s$ and $\tilde{y}' = y'/l_s$. The term S in this equation is modified as

$$S(\tilde{y}) = \frac{2}{\beta+1}\left[\zeta_0(\tilde{y}) - \frac{\zeta_1^2(\tilde{y})}{\zeta_2(\tilde{y})}\right], \tag{23}$$

with $\beta = \sqrt{l_a/l_s} = \sqrt{\tau_a/\tau_s}$ and

$$\zeta_k(\tilde{y}) = \overline{[\sin^k\varphi e^{-\tilde{y}/\beta\sin\varphi}]_+}. \tag{24}$$

The modified kernel K is given by Eq. (17) with

$$\begin{aligned} K_0(\tilde{y},\tilde{y}') &= \beta^{-1}\overline{[e^{-|\tilde{y}-\tilde{y}'|/\beta\sin\varphi}/\sin\varphi]_+} \\ &\quad + \beta^{-1}\frac{\beta-1}{\beta+1}\overline{[e^{-(\tilde{y}+\tilde{y}')/\beta\sin\varphi}/\sin\varphi]_+}, \\ K_1(\tilde{y},\tilde{y}') &= \beta^{-1}\mathrm{sgn}(\tilde{y}-\tilde{y}')\overline{[e^{-|\tilde{y}-\tilde{y}'|/\beta\sin\varphi}]_+} \\ &\quad + \beta^{-1}\frac{\beta-1}{\beta+1}\overline{[e^{-(\tilde{y}+\tilde{y}')/\beta\sin\varphi}]_+}, \end{aligned} \tag{25}$$

and with $\zeta_k(\tilde{y})$ of Eq. (24). Finally, Eq. (20) is modified by multiplying the integral term by β^{-1} and using there $\zeta_0(\tilde{y})$ of Eq. (24). If $l_a = l_s = l$ ($\beta = 1$), the problem is reduced to the one described by Eqs. (15)–(20). The presence of the energy-dependent factor β in the modified equations makes the energy averaging in the modified Eq. (20) essential, in contrast to the initial Eq. (20). However, if energy dependence of β is neglected, the boundary conductance $\mathcal{G}$ again does not depend on temperature, energy spectrum, and scattering time τ_s, although the dependence of $\mathcal{G}$ on β remains. The results of numerical calculations of the potential distribution for degenerate 2D electron gas is shown in Fig. 3, along with the dependence of the conductance on l_a/l_s. Increasing the ratio l_a/l_s brings the conductance closer to its upper bound, which is expectable since the total relaxation rate $\tau_s^{-1} + \tau_a^{-1}$ decreases. However, this also increases the width of the Knudsen layer. The transport properties of the hydrodynamic state beyond the Knudsen layer are governed only by the length l_s entering the expression for dynamic viscosity, $\eta = n\langle pl_s\rangle/(d+2)$. Indeed, the viscosity is determined by the relaxation time of the second angular harmonic of the distribution function, and this harmonic belongs to the symmetric set including all even harmonics. Thus, in contrast to the boundary conductance, the hydrodynamic transport in the bulk is not sensitive to whether the collision integral is given

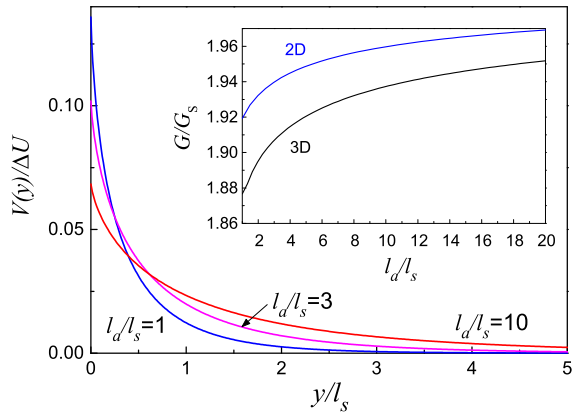

FIG. 3. Distribution of electrochemical potential in the Knudsen layer for 2D systems in the case of modified relaxation-time approximation for the collision integral described by the two-time model of Eq. (21). The inset shows the dependence of the boundary conductance on the ratio of relaxation lengths for antisymmetric and symmetric parts of the distribution function.

by Eq. (13) or Eq. (21), provided that both l_s and l_a are smaller than the other characteristic lengths.

The above consideration shows that electron scattering in the Knudsen layer produces a numerically small relative deviation of the boundary conductance from the approximate result of Eq. (10). The use of the improved model of electron-electron collision integral makes this deviation even smaller. This observation brings much credit to the method applied in derivation of Eq. (10). A similar method, with the difference that the hydrodynamic form of $g^-_{\mathbf{p}}$ approximates $g^-_{\mathbf{p}}(0)$ in the expression for the momentum flux density rather than the current density, has been applied to calculation of the slip length in the hydrodynamic boundary condition for tangential current, producing the results that are very close to those obtained in the detailed calculations taking into account electron collisions in the Knudsen layer [44]. Below, this method is applied in order to find the correction to the boundary conductance caused by a finite curvature of the boundary. The consideration is limited to 2D systems. The hydrodynamic description of the boundary implies that possible variation of the curvature occurs on a large scale compared to the Knudsen layer width. Thus, one can consider a piece of boundary with a constant curvature C which is positive for convex boundary and negative for concave boundary. In contrast to the case of flat boundary, the normal current density j_n near the curved boundary depends on the normal (radial) coordinate, in order to satisfy the current continuity, see also Sec. III. As a result, the viscous stress is generated in the bulk, so the distribution function there acquires an additional contribution proportional to $Q_{\alpha\beta}$, see Eq. (5). Calculating $Q_{\alpha\beta}$ in the hydrodynamic regime as described after Eq. (5), one obtains, instead of Eq. (7),

$$g^-_{\mathbf{p}} = eV - (p/en)j_n \sin\varphi - C(p\upsilon\tau/en)j_n \cos 2\varphi. \quad (26)$$

where φ denotes the angle of momentum with respect to the tangent to the boundary, which is reduced to the angle φ of the previous consideration if the curvature goes to zero. Applying Eq. (26) in Eq. (8), one gets

$$\frac{\mathcal{G}}{\mathcal{G}_S} = \frac{2}{1 + (4/3\pi)C\langle\upsilon\tau\rangle}, \quad (27)$$

which generalizes Eq. (10) to the case of 2D systems with curved contact boundaries. The convex boundary decreases the conductance, while the concave boundary increases it. Within the simplest model of the collision integral given by Eqs. (12) and (13), the length $\upsilon\tau$ is identified with $l \simeq l_e$, whereas in the modified model of Eq. (21) $\upsilon\tau = l_s$. At low temperatures, when the electron gas is degenerate, this length can be expressed through the viscosity according to $\langle\upsilon\tau\rangle = 4\eta/np_F$, where p_F is the Fermi momentum. The correction due to the curvature is parametrically small, because the product $|C|l$ must be small in the hydrodynamic transport regime. Nevertheless, this correction may become more important than the small numerical correction proportional to the difference $1-\alpha$. To take into account both these corrections, one may use the following expression:

$$\frac{\mathcal{G}}{\mathcal{G}_S} = \frac{2}{\alpha^{-1} + (4/3\pi)C\langle\upsilon\tau\rangle}. \quad (28)$$

When applying Eq. (28), one should neglect the terms containing double smallness $\propto (1-\alpha)C\langle\upsilon\tau\rangle$, since such terms are beyond the accuracy of the approximation.

III. TRANSPORT IN MICROSTRUCTURES

The results of the previous section can be applied for calculation of the conductance of various microstructures with contacts. In this section, the simplest examples of two-terminal devices are considered, where the electron transport can be described as well by solving the Boltzmann kinetic equation in a straightforward way. The kinetic equation approach makes it possible to study different transport regimes and transitions between them, and to link such results to those following from the above theory. The consideration below is limited to 2D systems, and the electron-electron collision integral is described by Eq. (13). The case of degenerate electron gas is studied, so the characteristic lengths l_e and l_{tr} appearing in the theory correspond to $\varepsilon = \varepsilon_F$ and have the direct meaning of the mean free path lengths.

Consider first the system of flat geometry shown in Fig. 1(c). Although it is implied that the device has a finite width W along Ox, the presence of the side walls is not essential as it is assumed that electrons are specularly reflected from these walls. In this case, the device behaves like an infinitely wide one, and its conductance in the ballistic limit is equal to the Sharvin conductance. The current flows along Oy and the current density $j_n = j_y$ does not depend on coordinates, whereas the electrochemical potential depends only on y. In the hydrodynamic regime, specular reflection is equivalent to the no-stress boundary condition, $\nabla_x j_y = 0$ at the side walls, which is satisfied automatically because the current density is constant. As there are no current density gradients, the linearized Navier-Stokes equation describing the current in the bulk of the system is reduced merely to the ohmic relation between the current density and the gradient of electrochemical potential in the bulk: $j_y = -\sigma_0 \nabla_y V(y)$, where σ_0 is the Drude conductivity. Thus, $\nabla_y V(y)$ is constant, and

the total resistance of the system is determined as a resistance in series, formed by the sum of two equal boundary resistances, $\mathcal{R}_0 = \mathcal{R}_1 = (2\alpha G_S)^{-1}$, and the bulk ohmic resistance. The latter is limited by momentum-relaxing scattering and is equal to $\mathcal{R}_{\rm bulk} = \sigma_0^{-1} L/W$, where L is the distance between the contacts. In 2D systems with degenerate electron gas, $\sigma_0 = e^2 n l_{tr}/\hbar k_F$, $G_S = {\rm g} e^2 k_F W/2\pi^2\hbar$, and $n = {\rm g} k_F^2/4\pi$, where k_F is the Fermi wavenumber and g is the degeneracy factor of electron states (e.g., g = 2 in GaAs and g = 4 in graphene). Then $\mathcal{R}_{\rm bulk} = G_S^{-1} 2L/\pi l_{tr}$, and the total resistance of the device is

$$\mathcal{R} = G_S^{-1}\left[\frac{1}{\alpha} + \frac{2}{\pi}\frac{L}{l_{tr}}\right], \tag{29}$$

where $\alpha \simeq 0.96$ according to the results of the previous section. Since $\alpha < 1$, such a device can never be superballistic, even if the momentum-relaxing scattering is absent. Thus, the momentum-conserving scattering alone increases the resistance of the system shown in Fig. 1(c), making it larger than the Sharvin resistance G_S^{-1}.

The expression for the resistance in the form similar to Eq. (29) remains valid for arbitrary l_e, l_{tr}, and L. This general case can be investigated by solving the kinetic equation. The nonequilibrium part of the distribution function is again governed by Eq. (14), with the boundary condition at $y = 0$ given by Eq. (6). Accordingly, at the right side $y = L$, the boundary condition is $g_{\mathbf{p}}^-|_{y=L} = eU_0$. If the point of zero electrochemical potential is chosen in the middle of the device, $y = L/2$, and the total applied voltage is defined as $U = U_1 - U_0$, the whole set of the boundary conditions is written as

$$g_\varphi^+(0) = eU/2,\ g_\varphi^-(L) = -eU/2. \tag{30}$$

The solution of the Cauchy problem defined by Eq. (14) and the boundary conditions of Eq. (30) is facilitated by the observation that $g_\varphi(y)$ can be represented in the form $g_\varphi(y) = h_\varphi(y) - (y - L/2)g_y/l_{tr}$, where $h_\varphi(y)$ satisfies Eq. (14) with $l_e = l$, i.e., with zero momentum-relaxing scattering, $l_{tr} \to \infty$. Accordingly, the boundary conditions for h_φ are modified by the formal substitution $eU \to eU - g_y L/l_{tr}$ so that $I = GU = G^*(U - g_y L/e l_{tr})$, where G^* is the effective conductance for the problem with zero momentum-relaxing scattering rate $1/l_{tr}$ and enhanced momentum-conserving scattering rate, $1/l_e \to 1/l_e + 1/l_{tr} \equiv 1/l$. Since $g_y = (2/\pi)e j_y/\mathcal{G}_S = (2/\pi)(G/G_S)eU$, the total resistance $\mathcal{R} = 1/G$ is given by Eq. (29), where α is replaced by G^*/G_S. The problem of finding G^* is described by Eq. (14) with $l_e = l$ and boundary conditions Eq. (30). It is reduced to solution of an integral equation similar to Eq. (15), see Appendix A. The ratio G^*/G_S depends on a single parameter, the Knudsen number K, defined here as ${\rm K} \equiv l/L$. In the ballistic limit, ${\rm K} \to \infty$, $G^* = G_S$. In the hydrodynamic limit, ${\rm K} \to 0$, $G^*/G_S = \alpha \simeq 0.96$.

In summary, the resistance of the system in Fig. 1(c) in the general case is given by

$$\mathcal{R} = \mathcal{R}^* + \frac{2}{\pi} G_S^{-1}\frac{L}{l_{tr}}, \tag{31}$$

where $\mathcal{R}^* \equiv 1/G^*$ is determined from Eqs. (A3)–(A7). In the hydrodynamic transport regime, when $l_e \ll l_{tr}$ and $l_e \ll L$, the effective resistance $\mathcal{R}^*$ is described as a sum of two boundary resistances and is equal to $(\alpha G_S)^{-1}$, so Eq. (31) is reduced to

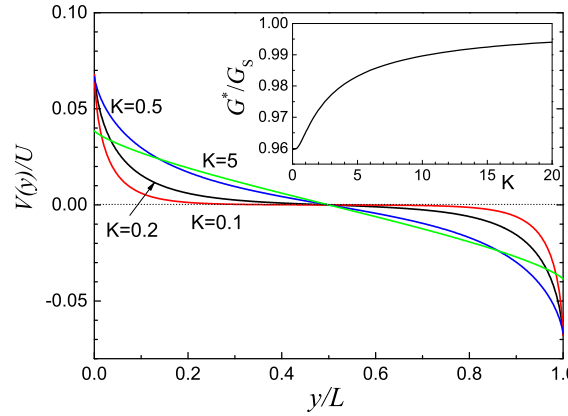

FIG. 4. Distribution of electrochemical potential along the 2D device with flat boundaries shown in Fig. 1(c), in the absence of momentum-relaxing scattering. The inset shows the dependence of the conductance on the Knudsen number ${\rm K} \equiv l/L$.

Eq. (29). The ratio G^*/G_S changes from 0.96 to 1 as the length l increases. The dependence of this ratio on the Knudsen number is shown in Fig. 4, which also demonstrates the potential profiles for different K in the absence of momentum-relaxing scattering. In the hydrodynamic regime, ${\rm K} \ll 1$, half of the total potential drops near each boundary, while in the bulk the potential is constant. When K increases above 1, the potential profile approaches a linear one, and the potential drop caused by the momentum-conserving scattering decreases.

Consider now the 2D Corbino disk system, Fig. 1(d), where the conducting layer is placed between the circular contact boundaries with radii R_1 (inner) and R_0 (outer). In the absence of magnetic field, only the radial flow with current density j is present, and all macroscopic quantities depend on the radial coordinate r. The continuity equation $\nabla \cdot \mathbf{j} = 0$ assumes the form

$$\nabla_r j(r) + j(r)/r = 0, \tag{32}$$

so that $j(r) = I/2\pi r$, where I is the total current. This property leads to disappearance of the viscous force, which means that the term proportional to the viscosity does not enter the Navier-Stokes equation [28], similar as in the case of the device with flat boundaries studied above. However, due to finite curvature of the boundaries, the current generates the viscous stress not only in the Knudsen layers, but also in the bulk of the system. The absence of the viscous term reduces the Navier-Stokes equation to the ohmic relation $j(r) = -\sigma_0 \nabla_r V(r)$ leading to the well-known logarithmic dependence of the electrochemical potential in the bulk: $V(r) = V(R_0) - I\ln(r/R_0)/2\pi\sigma_0$, so the bulk resistance is $\mathcal{R}_{\rm bulk} = \ln(R_0/R_1)/2\pi\sigma_0$. The resistances of the outer and inner boundaries are $\mathcal{R}_0 = (2\pi R_0 \mathcal{G})^{-1}$ and $\mathcal{R}_1 = (2\pi R_1 \mathcal{G})^{-1}$, because the contact widths are equal to circumference of the boundaries. The curvatures of these boundaries are $-1/R_0$ and $1/R_1$. Thus, according to Eq. (28) with $\langle v\tau\rangle = l$, the sum of the resistances is

$$\mathcal{R}^* = \mathcal{R}_0 + \mathcal{R}_1 = G_S^{-1}\left[\frac{b+1}{2b\alpha} + \frac{2(b^2-1)}{3\pi b}{\rm K}\right], \tag{33}$$

where $b \equiv R_0/R_1$. The Knudsen number is defined here as $\mathrm{K} \equiv l/R_0$. The ballistic conductance of the Corbino disk device is equal to the Sharvin conductance [35]

$$G_S = 2\pi R_1 \mathcal{G}_S = \mathrm{g} e^2 k_F R_1/\pi\hbar, \tag{34}$$

which is proportional to the circumference of the inner contact as the ballistic electron flow is limited by the smallest circumference. One can also derive Eq. (34) from the kinetic equation in the ballistic limit (see Appendix B). By adding the resistances in series, one obtains the total resistance of the device in the hydrodynamic transport regime,

$$\mathcal{R} = \mathcal{R}^* + \frac{2}{\pi} G_S^{-1} \frac{R_1 \ln b}{l_{tr}}. \tag{35}$$

In contrast to the device with flat boundaries, the Corbino disk device can be superballistic, i.e., $\mathcal{R}$ can be smaller than the Sharvin resistance G_S^{-1}. The contribution to $\mathcal{R}^*$ due to boundary curvatures, given by the second term in the right-hand side of Eq. (33), coincides with the resistance calculated in Ref. [28] up to a numerical coefficient 2/3. Note, however, that the authors of Ref. [28] considered a problem when this contribution was the main one, while in the present theory it represents a small correction to the total resistance. If the momentum-relaxing scattering is absent, the total resistance is equal to the sum of the boundary contact resistances, $\mathcal{R} = \mathcal{R}^*$, and the potential in the bulk of the device is constant, $V(r) = V_{\mathrm{bulk}}$ [28]. Since $V_{\mathrm{bulk}} = \mathcal{R}_0 I$,

$$\frac{V_{\mathrm{bulk}}}{U} = \frac{1 - 4\mathrm{K}/3\pi}{(b+1)(1 + 4\mathrm{K}(b-1)/3\pi)}. \tag{36}$$

In the hydrodynamic limit, $\mathrm{K} \to 0$, Eqs. (33) and (36) assume the simple forms $\mathcal{R}^* = G_S^{-1}(b+1)/2b\alpha$ and $V_{\mathrm{bulk}}/U = 1/(b+1)$. The inequality $\mathrm{K} \ll 1$ is the necessary condition for the validity of hydrodynamic description of the transport. The sufficient conditions are $l \ll \min\{R_1, R_0 - R_1\}$ and $l_e \ll l_{tr}$.

Equation (35) with properly redefined $\mathcal{R}^*$ remains valid in the case of arbitrary l_e, l_{tr}, R_0, and R_1. To prove this statement, one needs to consider the kinetic equation. In the Corbino geometry, the function $g_{\mathbf{p}}(\mathbf{r})$ can be written as $g_\varphi(r)$, where φ now denotes the angle of momentum with respect to the tangent to the inner boundary. The angle φ has the same meaning as before if the radial direction is identified with the Oy axis. Equation (11) for $g_\varphi(r)$ assumes the form

$$\sin\varphi \nabla_r g_\varphi(r) + \frac{1}{r}\cos\varphi \frac{\partial g_\varphi(r)}{\partial\varphi} + \frac{g_\varphi(r)}{l} = \frac{\bar{g}(r)}{l} + \frac{A\sin\varphi}{l_e r}, \tag{37}$$

where the radial (the only nonzero) component of the vector $\mathbf{g}$ is written as A/r, since it is proportional to the current density. The constant A is expressed as $A = I/\pi e D_F v_F$, where D_F and v_F are the density of states and group velocity at the Fermi level. Similar as above, it is convenient to decompose $g_\varphi(r)$ into $g_\varphi^+ = g_\varphi$ and $g_\varphi^- = g_{2\pi-\varphi}$ defined in the angular interval $\varphi \in [0, \pi]$ and describing the particles moving from the center and towards the center, respectively. Then, the in-flow boundary conditions for $g_\varphi(r)$ are

$$g_\varphi^+(R_1) = eU, \; g_\varphi^-(R_0) = 0, \tag{38}$$

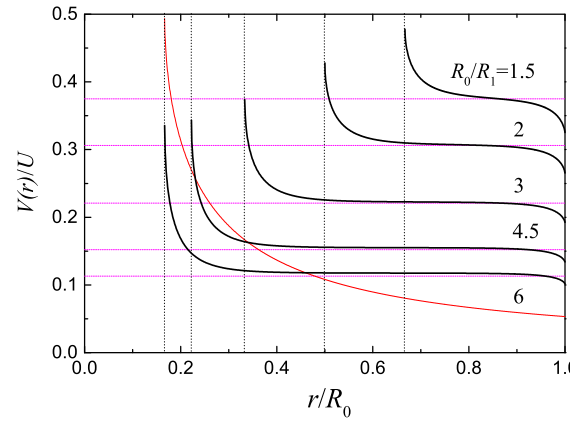

FIG. 5. Bulk potential profiles for Corbino disk devices with different ratios $b = R_0/R_1$ from 1.5 to 6 for $\mathrm{K} \equiv l/R_0 = 0.1$ in the absence of momentum-relaxing scattering. For comparison, thin red line shows the potential profile for purely ballistic transport, $V(r) = (U/\pi)\arcsin(R_1/r)$, at $b = 6$. The horizontal lines show the magnitude of the flat part V_{bulk} according to Eq. (36). The vertical lines indicate the positions of the inner boundary, $r = R_1$.

where the point of zero potential is chosen at the outer electrode. The Boltzmann kinetic equation with boundary conditions of Eq. (38) has been used in the analysis of experimental data for the Corbino disk with $R_0/R_1 = 4.5$ in Ref. [35]. The function $g_\varphi(r)$ is representable in the form $g_\varphi(\rho) = h_\varphi(r) - A\ln(r/R_0)/l_{tr}$, where $h_\varphi(r)$ satisfies Eq. (37) with $l_e = l$. Accordingly, the boundary conditions for h_φ are modified by the substitution $eU \to eU - A\ln b/l_{tr}$. This leads to Eq. (35), where the effective resistance $\mathcal{R}^*$ is now found by solving the problem described by Eqs. (37) and (38) with $l_e = l$, which is formally equivalent to the transport problem with zero momentum-relaxing scattering rate and enhanced momentum-conserving scattering rate, $1/l_e \to 1/l_e + 1/l_{tr} \equiv 1/l$ [35]. This problem is solved by the method of characteristics as described in Appendix B.

The potential profiles for Corbino disks with different b, calculated at $\mathrm{K} = 0.1$ in the absence of momentum-relaxing scattering, when $\mathcal{R} = \mathcal{R}^*$, are shown in Fig. 5. They demonstrate almost flat electrochemical potentials in the middle regions and rapid change of the potentials in the Knudsen layers of width $\simeq l$ near the boundaries. The magnitudes of the flat parts of the potentials decrease with increasing b and are in good agreement with those given by Eq. (36). If $R_0 - R_1 \ll R_0$, the behavior of the potential in Corbino devices approaches to that shown in Fig. 4, since the curvature effect becomes no longer important. To account for the momentum-relaxing scattering, one should add the contribution $I\ln(R_0/r)/2\pi\sigma_0 = IG_S^{-1}(2R_1/\pi l_{tr})\ln(R_0/r)$ to the potential profile. The results presented are consistent with the data obtained by experimental imaging of the potential distribution in the Corbino device [35]. The resistance $R(r)$ found in these measurements is related to the potential calculated here as $R(r) = V(r)/I$, within the accuracy of spatial smearing due to a finite resolution of the imaging. The scale of this smearing, 1 μm, is larger than the width of the Knudsen layer in the hydrodynamic transport regime. This fact, together with the nonideal transmission at the contact interfaces of real

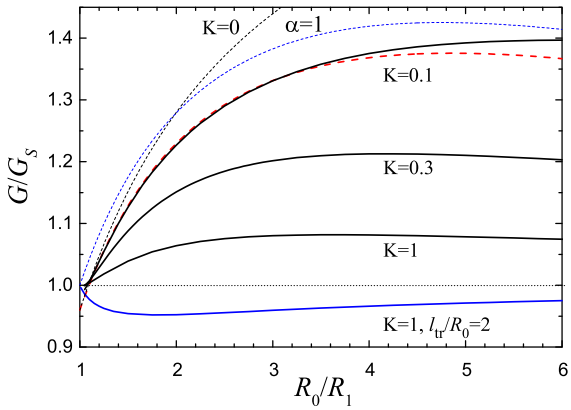

FIG. 6. Conductance of Corbino disk devices as a function of the ratio R_0/R_1. Three upper plots (black-solid lines) are calculated in the absence of momentum-relaxing scattering, $l_{tr} \to \infty$, and the lower plot corresponds to $l_{tr} = l_e = 2l = 2R_0$. The dashed lines show the approximate results according to Eq. (33): K = 0.1 and $\alpha = 0.96$ (red); K = 0.1 and $\alpha = 1$ (blue); and K = 0 and $\alpha = 0.96$ (black).

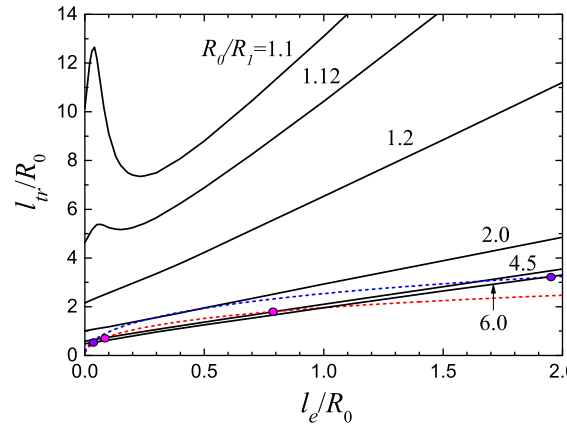

FIG. 7. The borders of superballistic behavior for Corbino disks with different ratios $b = R_0/R_1$ (indicated) in the space of parameters l_e and l_{tr}. The lines correspond to $G = G_S$. In the regions above the lines the transport is superballistic, $G > G_S$. Red and blue dashed lines show the dependence of l_{tr}/R_0 on l_e/R_0 when temperature is changed, plotted by using the experimental details of two devices with $b = 4.5$ and $b = 6$ from Ref. [35]. The intersection points of these plots with the lines $G = G_S$ for $b = 4.5$ and $b = 6$ are shown.

Corbino devises [35], hinders a detailed quantitative comparison of the theoretical and experimental potential profiles.

The dependence of the conductance on the ratio R_0/R_1 is shown in Fig. 6. In the absence of momentum-relaxing scattering, when $\mathcal{R} = \mathcal{R}^*$, the numerical result at K = 0.1 is in good agreement with the approximate result given by Eq. (33). The deviation in the region of large R_0/R_1 occurs because the curvature-induced correction is no longer small, $l/R_1 = b\mathrm{K} \sim 1$, and Eq. (33) loses its validity. Thin dashed lines in Fig. 6 show the results of more crude approximations that neglect either the effect of scattering in the Knudsen layer ($\alpha = 1$) or the curvature effect [$C = 0$ in Eq. (28) or, equivalently, K = 0 in Eq. (33)]. In general, the conductance is the highest when the momentum-conserving scattering is strong and the momentum-relaxing scattering is weak. The superballistic conductance $G > G_S$ does not require the hydrodynamic transport regime and can be observed even at $l_e > R_0$ if the momentum-relaxing scattering is weak enough. To obtain a considerable superballistic effect, it is preferable to use the devices with $R_0/R_1 > 2$.

The important question about the existence of superballistic conductance depending on the parameters of the problem is addressed in more detail in Fig. 7. It shows the lines separating the regimes $G > G_S$ and $G < G_S$ in the parameter space. These lines are nearly straight if R_1 is not too close to R_0. Otherwise, when $b - 1$ is comparable to $1 - \alpha$, the shape of the border lines is essentially different from linear at small l_e/R_0. Regardless of the value of R_0/R_1, the superballistic conductance requires $l_{tr} > l_e$, that is the rate of electron-electron scattering must be higher than the rate of momentum-relaxing one. In the hydrodynamic limit, $l_e/R_0 \to 0$, the superballistic conductance requires $l_{tr}/R_0 > (2/\pi)\ln b/[b - (b+1)/2\alpha]$ and exists at $b > 1/(2\alpha - 1)$. For finite l_e, however, the superballistic conductance may exist even at $b < 1/(2\alpha - 1)$, although in this case the conductance only slightly exceeds G_S. The characteristic lengths l_{tr} and l_e are varied by the temperature T. For a degenerate fermion gas,

$$l_e \simeq \gamma v_F \hbar \varepsilon_F / T^2, \tag{39}$$

where γ can be approximated by a numerical constant of order unity. On the other hand, $l_{tr} \sim 1/T$ if the main mechanism of momentum-changing scattering is the interaction of electrons with acoustic phonons and T exceeds Bloch-Grüneisen temperature. Therefore, by changing the temperature one moves in the parameter space along the square root line $l_{tr} \sim \sqrt{l_e}$, which may intersect the border lines shown in Fig. 7 in two points. This means that the superballistic conductance is expected to exist in a temperature interval corresponding to the interval between these points. In the presence of a considerable electron-electron scattering, the resistance should have a minimum as a function of T that correlates with Eq. (39) and depends on the system size, like in the Gurzhi effect [11]. Such a behavior was recently observed [35] in graphene Corbino disks. Using the device dimensions $R_0 = 9$ μm and $R_1 = 2$ μm, density $n = 4.5 \times 10^{11}$ cm^{-2}, graphene Fermi velocity $v_F = 10^8$ cm/s, and the temperature dependence $l_{tr}[\mu\mathrm{m}] = (0.016 + 0.0015T[\mathrm{K}])^{-1}$, which gives a sufficiently accurate approximation of the one extracted from the experimental data (see Supplemental Material for [35]), one may plot the dependence of l_{tr} on l_e. This dependence, obtained with $\gamma = 1$ in Eq. (39), is also shown in Fig. 7. According to the calculations, the superballistic transport should be observed in the temperature interval between 31 K and 93 K with the minimum of the resistance near 60 K. The temperature dependence of the resistance shown in Fig. 8 is consistent with the experimental results, see the next paragraph for more details. The experimental data suggest that the hydrodynamic regime in the bulk is reached approximately at $T = 140$ K. According to Eq. (39) with $\gamma = 1$, at this temperature $l_e \simeq 0.36$ μm, which, indeed, is much smaller than $l_{tr} \simeq 4.5$ μm and considerably smaller than the inner contact radius $R_1 = 2$ μm. In the case of the sample with a smaller electron density, $n = 3.3 \times 10^{11}$ cm^{-2}, also investigated in the experiment (see Supplemental Material for [35]), the calculated temperature interval shows only

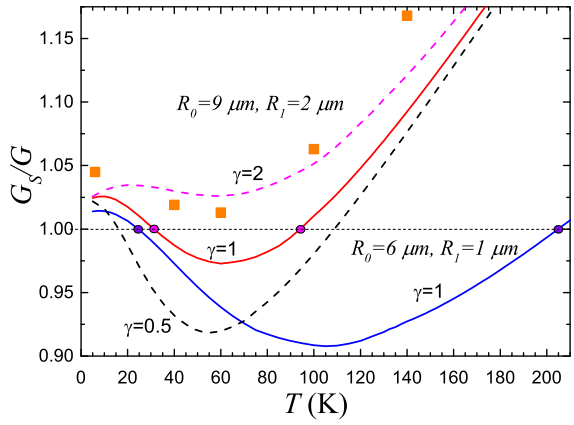

FIG. 8. Calculated temperature dependence of the normalized resistance G_S/G for two Corbino disk devices studied in Ref. [35]. For the device with $R_0 = 9$ μm and $R_1 = 2$ μm, the plots with $\gamma = 0.5$ and $\gamma = 2$ are included to show sensitivity of the resistance to the strength of electron-electron interaction. Squares show the experimental data extracted from Ref. [35] as described in the text.

a slight change, from 26 K to 99 K. The theoretical results are sensitive to the numerical constant γ, as demonstrated in Fig. 8. With $\gamma = 2$ in Eq. (39) (weaker electron-electron interaction), the transport is no longer superballistic for a given device, although the minimum in the temperature dependence of the resistance persists. With $\gamma = 0.5$ in Eq. (39) (stronger electron-electron interaction) the temperature interval for superballistic transport is considerably broader, as well as the depth of the resistance minimum. The position of the minimum is only slightly shifted when γ is changed. The authors of Ref. [35] also studied a smaller Corbino device with $R_0 = 6$ μm and $R_1 = 1$ μm (see Supplemental Material for [35]). For this device, the intervals of parameters, as well as the interval of temperatures corresponding to superballistic transport increase considerably, as shown in Figs. 7 and 8, and the resistance minimum is expected around 105 K. As the experimental data for this particular device are limited, a detailed comparison with experiment is given below for the device with $R_0 = 9$ μm and $R_1 = 2$ μm ($b = 4.5$).

The measured [35] resistance of the Corbino devices is higher than the theoretical one because the contacts do not transmit electrons perfectly. In particular, at low temperatures, when the transport is nearly ballistic, the theory (Fig. 8) gives the normalized resistance $G_S/G \simeq 1.025$ for the device with $b = 4.5$, while the corresponding experimental value is 1.42. To exclude the contact contributions, the authors of Ref. [35] introduced the quantity $R_{\rm bulk}/R_{sh}^{in}$ (R_{sh}^{in} denotes the Sharvin resistance, the same as G_S^{-1}) derived from the total measured resistance by subtracting the contact resistances for the inner and the outer contacts. These resistances have been found by comparing the measured potential profile at $T = 6$ K with the sum of the theoretically known ballistic potential profile $V(r) = (U/\pi)\arcsin(R_1/r)$ and two smeared step functions representing the contact contributions. Thus, for the ideal (perfectly transmitting) contacts assumed in the present paper, the inner and outer contact resistances would be $G_S^{-1}/2$ and $G_S^{-1}\pi^{-1}\arcsin(1/b) \simeq G_S^{-1}/\pi b$, respectively. The relation between the total normalized resistance of the ideal Corbino device and the quantity $R_{\rm bulk}/R_{sh}^{in}$ specified in Ref. [35] is reduced to a shift $G_S/G \simeq R_{\rm bulk}/R_{sh}^{in} + 1/2 + 1/\pi b \simeq R_{\rm bulk}/R_{sh}^{in} + 0.57$. The experimental points shifted in this way are shown in Fig. 8 by the squares. The position of the resistance minimum near 60 K is in good agreement with the experiment. The absolute values of the calculated G_S/G are not far from the experimental ones, and can be put within 10% of relative deviation from the experimental ones by variation of the parameter γ. Taking into account that the contact resistances, and hence the quantity $R_{\rm bulk}/R_{sh}^{in}$, are determined within the accuracy of 10% [35], one can say that the theory satisfactory describes the experiment. This agreement also indicates that the conductance of high-quality Corbino devices with nearly perfectly transmitting contacts can exceed the ballistic limit G_S, so the experimental results provide a convincing proof for the possible superballistic transport in these systems.

In should be emphasized, however, that the contact resistances introduced in Ref. [35] are different from the boundary resistances described in this paper. These boundary resistances are defined in the hydrodynamic transport regime when the contacts can be considered separately from each other. The sum of the inner and outer boundary resistances is given by Eq. (33), and the total resistance is given by Eq. (35) by adding the bulk resistance to this sum.

IV. SUMMARY

In this paper, the classical transport properties of electron systems contacted to perfectly conducting electrodes (leads) have been studied. If the electron gas in the bulk is in the hydrodynamic transport regime, there exists a thin Knudsen layer separating the lead from the hydrodynamic electron state [Fig. 1(b)]. The interface between the lead and this state can be characterized by the conductance per unit contact area $\mathcal{G}$, which is intrinsically superballistic: $\mathcal{G} = 2\alpha\mathcal{G}_S$, where $\mathcal{G}_S$ is the Sharvin conductance per unit area and α is a numerical constant slightly smaller than unity. Remarkably, within the elastic relaxation-time approximation for electron-electron collision integral, which is often applied in theoretical description of electron transport, α depends only on the dimensionality of the system and is approximately equal to 0.96 for 2D systems and 0.94 for 3D systems. Application of the modified double-time approximation for electron-electron collision integral [40], which takes into account the difference in relaxation times for even and odd angular harmonics of the distribution function, brings α closer to unity (Fig. 3). The correction to $\mathcal{G}$ due to finite curvature of the contact boundary also has been found. It is shown that $\mathcal{G}$ decreases for the convex boundary and increases for the concave boundary.

Based on these results, the conductance of highly symmetric 2D microstructures [Figs. 1(c) and 1(d)], where the current is always normal to the contact boundaries, has been described. The important example of this kind is the Corbino disk device, whose conductance G can exceed the Sharvin conductance G_S owing to the superballistic contact property of the device boundaries. The conductance of Corbino disks has been calculated as well by means of numerical solution of the Boltzmann kinetic equation, which describes different transport regimes and transitions between them, depending

on the characteristic lengths of the problem. In the hydrodynamic transport regime, when the Knudsen number K is small, the calculated conductance and the electrochemical potential in the bulk are in good agreement with the simple analytical formulas obtained from the consideration of a single contact boundary (Figs. 5 and 6). The kinetic equation approach shows that the superballistic conductance of Corbino disks does not require the hydrodynamic transport regime, although the domination of electron-electron scattering over the momentum-relaxing scattering is a necessary requirement. The map in the parameter space, indicating the regions with superballistic conductance $G > G_S$, has been presented (Fig. 7). By considering the dependence of electron-electron and momentum-relaxing mean free path lengths on temperature, it is concluded that the superballistic conductance in Corbino disks can be observed within a certain interval of temperatures. The general behavior of G as well as the position of the temperature minimum of the resistance G^{-1} are in agreement with experimental results [35].

The calculation of the conductance standing in Eq. (1) is important by itself, without regard to the specific problem of superballistic transport. Indeed, Eq. (1) relates the normal current density to the voltage of the contact and should be considered as a hydrodynamic boundary condition for the normal current density at the current-penetrable boundary. On the other hand, the tangential current density $\mathbf{j}_t$ is related to its normal derivative at the boundary by Maxwell's boundary condition, $\mathbf{j}_t = l_S \nabla_n \mathbf{j}_t$ [44–46], which is usually applied to the hard-wall boundaries, where the normal current is zero. The tangential current density at the current-penetrable boundaries can be as well described by Maxwell's boundary condition derived in the fully diffuse limit, which corresponds to the slip lengths $l_S = 0.582 l_e$ and $l_S = 0.637 l_e$ for degenerate 3D and 2D fermion gases, respectively [44]. By combining Maxwell's boundary conditions with Eq. (1), one obtains a full set of hydrodynamic boundary conditions, describing both tangential and normal current for both hard-wall and current-penetrable boundaries. These boundary conditions, together with the Navier-Stokes equation, form a Cauchy problem for determination of the current density and potential distribution in various microstructures in the hydrodynamic transport regime, which is important for applications, in particular, for development of viscous electronics [22].

APPENDIX A

The solution of Eq. (14) with $l_e = l$ and boundary conditions Eq. (30) is

$$g_\varphi^+(y) = g_y(1 - e^{-y/l\sin\varphi})\sin\varphi + \frac{eU}{2}e^{-y/l\sin\varphi} + \int_0^y \frac{dy'}{l\sin\varphi} e^{(y'-y)/l\sin\varphi}\bar{g}(y'), \tag{A1}$$

$$g_\varphi^-(y) = -g_y(1 - e^{(y-L)/l\sin\varphi})\sin\varphi - \frac{eU}{2}e^{(y-L)/l\sin\varphi} + \int_y^L \frac{dy'}{l\sin\varphi} e^{(y-y')/l\sin\varphi}\bar{g}(y'). \tag{A2}$$

With $\bar{g}(y) = \overline{[(g_\varphi^+ + g_\varphi^-)]}_+ = (2\pi)^{-1}\int_0^\pi d\varphi[g_\varphi^+(y) + g_\varphi^-(y)]$ and $g_y = 2\overline{[(g_\varphi^+ - g_\varphi^-)\sin\varphi]}_+ = \pi^{-1}\int_0^\pi d\varphi[g_\varphi^+(y) - g_\varphi^-(y)]\sin\varphi$, one gets an integral equation for $\bar{g}(y)$. Since $\bar{g}(y) = eV(y)$, this equation is written as an equation for the electrochemical potential,

$$V(\tilde{y}) = \frac{U}{2}\mathcal{S}(\tilde{y}) + \int_0^{L/l} d\tilde{y}\mathcal{K}(\tilde{y},\tilde{y}')V(\tilde{y}'), \tag{A3}$$

where the dimensionless coordinates $\tilde{y} = y/l$ and $\tilde{y}' = y'/l$ are used. In Eq. (A3),

$$\mathcal{S}(\tilde{y}) = \zeta_0^-(\tilde{y}) - \zeta_1^-(\tilde{y})\zeta_1^+(\tilde{y})/\zeta_2^+(\tilde{y}), \tag{A4}$$

$$\mathcal{K}(\tilde{y},\tilde{y}') = K_0(\tilde{y},\tilde{y}') - \frac{\zeta_1^-(\tilde{y})}{\zeta_2^+(\tilde{y})}K_1(\tilde{y},\tilde{y}'), \tag{A5}$$

K_0 and K_1 are given by Eq. (18), and

$$\zeta_k^\pm(\tilde{y}) = \overline{[\sin^k\varphi(e^{-\tilde{y}/\sin\varphi} \pm e^{(\tilde{y}-L/l)/\sin\varphi})]}_+. \tag{A6}$$

Once $V(y)$ is found, the ratio G^*/G_S is found from the expression

$$\frac{G^*}{G_S} = \frac{\pi\zeta_1^+(0)}{4\zeta_2^+(0)}\left[1 - \frac{2}{\zeta_1^+(0)}\int_0^{L/l} d\tilde{y}\zeta_0(\tilde{y})V(\tilde{y})/U\right]. \tag{A7}$$

where ζ_0 is given by Eq. (19). In the ballistic limit, $l/L \to \infty$, $G^* = G_S$. In the hydrodynamic limit, $l/L \to 0$, one has $\zeta_k^\pm = \zeta_k$, $\mathcal{S} = S$, $\mathcal{K} = K$, and Eq. (A3) becomes identical to Eq. (15) with $\Delta U = U/2$, reflecting the property that half of the total potential drops near each boundary. Since $\zeta_1(0) = 1/\pi$ and $\zeta_2(0) = 1/4$, Eq. (A7) is reduced to $G^*/G_S = \alpha$, where α is given by Eq. (20).

APPENDIX B

The solution of Eq. (37) with $l_e = l$ and boundary conditions Eq. (38) is

$$g_\varphi^+(\rho) = eU\theta(\rho_1 - |w|)e^{\psi_w(\rho_1)-\psi_w(\rho)} + \theta(|w| - \rho_1) \times \int_{\max\{\rho_1,|w|\}}^{\rho_0} d\rho' e^{-\psi_w(\rho)-\psi_w(\rho')}\left[\frac{\rho'\bar{g}(\rho')}{\psi_w(\rho')} - \frac{A}{l\rho'}\right] + \int_{\max\{\rho_1,|w|\}}^{\rho} d\rho' e^{-\psi_w(\rho)+\psi_w(\rho')}\left[\frac{\rho'\bar{g}(\rho')}{\psi_w(\rho')} + \frac{A}{l\rho'}\right], \tag{B1}$$

$$g_\varphi^-(\rho) = \int_\rho^{\rho_0} d\rho' e^{\psi_w(\rho)-\psi_w(\rho')}\left[\frac{\rho'\bar{g}(\rho')}{\psi_w(\rho')} - \frac{A}{l\rho'}\right], \tag{B2}$$

where the dimensionless quantities are introduced according to $\rho = r/l$, $\rho' = r'/l$, $\rho_0 = R_0/l$, $\rho_1 = R_1/l$, $w = \rho\cos\varphi$, and $\psi_w(\rho) = \sqrt{\rho^2 - w^2}$. The latter is related to φ as $\psi_w(\rho) = \rho\sin\varphi$. The solution satisfies the necessary requirements $g_0^+(\rho) = g_0^-(\rho)$ and $g_\pi^+(\rho) = g_\pi^-(\rho)$ expressing periodicity of $g_\varphi(\rho)$ and its continuity at $\varphi = \pi$. Applying $\bar{g}(\rho) = eV(\rho) = (2\pi)^{-1}\int_0^\pi d\varphi[g_\varphi^+(\rho) + g_\varphi^-(\rho)]$ and $A/r = \pi^{-1}\int_0^\pi d\varphi[g_\varphi^+(\rho) - g_\varphi^-(\rho)]\sin\varphi$, one obtains the integral

equation

$$V(\rho) = U\mathcal{L}(\rho) + \int_{\rho_1}^{\rho_0} d\rho' \mathcal{Q}(\rho, \rho') V(\rho'). \tag{B3}$$

The functions entering Eq. (B3) are

$$\mathcal{L}(\rho) = \mathcal{L}_0(\rho) + \mathcal{L}_1(\rho) Z_0(\rho)/[1 - Z_1(\rho)], \tag{B4}$$

$$\mathcal{Q}(\rho, \rho') = \mathcal{Q}_0(\rho, \rho') + \mathcal{Q}_1(\rho, \rho') Z_0(\rho)/[1 - Z_1(\rho)], \tag{B5}$$

$$\mathcal{L}_0(\rho) = \frac{1}{\pi} \int_0^{\rho_1} dw \frac{e^{\psi_w(\rho_1) - \psi_w(\rho)}}{\psi_w(\rho)}, \tag{B6}$$

$$\mathcal{L}_1(\rho) = \frac{2}{\pi} \int_0^{\rho_1} dw e^{\psi_w(\rho_1) - \psi_w(\rho)}, \tag{B7}$$

$$\mathcal{Q}_0(\rho, \rho') = \frac{1}{\pi} \int_0^{\rho_m} dw \frac{e^{-|\psi_w(\rho) - \psi_w(\rho')|} \rho'}{\psi_w(\rho)\psi_w(\rho')} + \frac{1}{\pi} \int_{\rho_1}^{\rho_m} dw \frac{e^{-\psi_w(\rho) - \psi_w(\rho')} \rho'}{\psi_w(\rho)\psi_w(\rho')}, \tag{B8}$$

$$\mathcal{Q}_1(\rho, \rho') = \frac{2}{\pi} \int_0^{\rho_m} dw \frac{e^{-|\psi_w(\rho) - \psi_w(\rho')|} \mathrm{sgn}(\rho - \rho') \rho'}{\psi_w(\rho')} + \frac{2}{\pi} \int_{\rho_1}^{\rho_m} dw \frac{e^{-\psi_w(\rho) - \psi_w(\rho')} \rho'}{\psi_w(\rho')}, \tag{B9}$$

$$Z_0(\rho) = \frac{1}{\pi} \int_{\rho_1}^{\rho_0} \frac{d\rho'}{\rho'} \left[\int_0^{\rho_m} dw \frac{e^{-|\psi_w(\rho) - \psi_w(\rho')|}}{\psi_w(\rho)} \times \mathrm{sgn}(\rho - \rho') - \int_{\rho_1}^{\rho_m} dw \frac{e^{-\psi_w(\rho) - \psi_w(\rho')}}{\psi_w(\rho)} \right], \tag{B10}$$

and

$$Z_1(\rho) = \frac{2}{\pi} \int_{\rho_1}^{\rho_0} \frac{d\rho'}{\rho'} \left[\int_0^{\rho_m} dw e^{-|\psi_w(\rho) - \psi_w(\rho')|} - \int_{\rho_1}^{\rho_m} dw e^{-\psi_w(\rho) - \psi_w(\rho')} \right], \tag{B11}$$

where $\rho_m = \min\{\rho, \rho'\}$. The conductance $G^* = 1/R^*$ is determined by the solution of Eq. (B3) as follows:

$$\frac{G^*}{G_S} = \frac{1 - (\pi/\rho_1) \int_{\rho_1}^{\rho_0} d\rho \rho \mathcal{L}_0(\rho) V(\rho)/U}{1 - \int_{\rho_1}^{\rho_0} d\rho \mathcal{L}_1(\rho)/\rho}. \tag{B12}$$

The conductance depends on the ratios R_0/l and R_1/l. In the ballistic limit, when $R_0/l \to 0$, the integral terms in Eq. (B12) go to zero as well and $G^* = G_S$, while Eq. (B3) is reduced to $V(\rho) = U\mathcal{L}_0(\rho)$ describing the potential distribution $V(r) = (U/\pi)\arcsin(R_1/r)$ [28,35]. In the hydrodynamic limit, when $l/R_1 \to 0$, $l/(R_0 - R_1) \to 0$, the relations $G^*/G_S = 2b\alpha/(b+1)$ and $V(r) = V_{\mathrm{bulk}} = U/(b+1)$ are restored.

[1] M. Müller, J. Schmalian, and L. Fritz, Graphene: A Nearly Perfect Fluid, Phys. Rev. Lett. **103**, 025301 (2009).

[2] R. Bistritzer and A. H. MacDonald, Hydrodynamic theory of transport in doped graphene, Phys. Rev. B **80**, 085109 (2009).

[3] A. V. Andreev, S. A. Kivelson, and B. Spivak, Hydrodynamic Description of Transport in Strongly Correlated Electron Systems, Phys. Rev. Lett. **106**, 256804 (2011).

[4] B. N. Narozhny, I. V. Gornyi, M. Titov, M. Schütt, and A. D. Mirlin, Hydrodynamics in graphene: Linear-response transport, Phys. Rev. B **91**, 035414 (2015).

[5] A. Lucas, J. Crossno, K. C. Fong, P. Kim, and S. Sachdev, Transport in inhomogeneous quantum critical fluids and in the Dirac fluid in graphene, Phys. Rev. B **93**, 075426 (2016).

[6] A. Principi, G. Vignale, M. Carrega, and M. Polini, Bulk and shear viscosities of the two-dimensional electron liquid in a doped graphene sheet, Phys. Rev. B **93**, 125410 (2016).

[7] A. Levchenko, H.-Y. Xie, and A. V. Andreev, Viscous magnetoresistance of correlated electron liquids, Phys. Rev. B **95**, 121301(R) (2017).

[8] A. Lucas, Stokes paradox in electronic Fermi liquids, Phys. Rev. B **95**, 115425 (2017).

[9] A. Lucas and S. A. Hartnoll, Kinetic theory of transport for inhomogeneous electron fluids, Phys. Rev. B **97**, 045105 (2018).

[10] A. Lucas and K. C. Fong, Hydrodynamics of electrons in graphene, J. Phys.: Condens. Matter **30**, 053001 (2018).

[11] R. N. Gurzhi, Minimum of resistance in impurity free conductors, Sov. Phys. JETP **17**, 521 (1963).

[12] M. J. M. de Jong and L. W. Molenkamp, Hydrodynamic electron flow in high-mobility wires, Phys. Rev. B **51**, 13389 (1995).

[13] G. M. Gusev, A. D. Levin, E. V. Levinson, and A. K. Bakarov, Viscous electron flow in mesoscopic two-dimensional electron gas, AIP Adv. **8**, 025318 (2018).

[14] P. S. Alekseev, Negative Magnetoresistance in Viscous Flow of Two-Dimensional Electrons, Phys. Rev. Lett. **117**, 166601 (2016).

[15] T. Scaffidi, N. Nandi, B. Schmidt, A. P. Mackenzie, and J. E. Moore, Hydrodynamic Electron Flow and Hall Viscosity, Phys. Rev. Lett. **118**, 226601 (2017).

[16] G. M. Gusev, A. D. Levin, E. V. Levinson, and A. K. Bakarov, Viscous transport and Hall viscosity in a two-dimensional electron system, Phys. Rev. B **98**, 161303(R) (2018).

[17] T. Holder, R. Queiroz, and A. Stern, Unified Description of the Classical Hall Viscosity, Phys. Rev. Lett. **123**, 106801 (2019).

[18] I. Torre, A. Tomadin, A. K. Geim, and M. Polini, Nonlocal transport and the hydrodynamic shear viscosity in graphene, Phys. Rev. B **92**, 165433 (2015).

[19] D. A. Bandurin, I. Torre, R. K. Kumar, M. Ben Shalom, A. Tomadin, A. Principi, G. H. Auton, E. Khestanova, K. S. Novoselov, I. V. Grigorieva *et al.*, Negative local resistance caused by viscous electron backflow in graphene, Science **351**, 1055 (2016).

[20] F. M. D. Pellegrino, I. Torre, A. K. Geim, and M. Polini, Electron hydrodynamics dilemma: Whirlpools or no whirlpools, Phys. Rev. B **94**, 155414 (2016).

[21] F. M. D. Pellegrino, I. Torre, and M. Polini, Nonlocal transport and the Hall viscosity of two-dimensional hydrodynamic electron liquids, Phys. Rev. B **96**, 195401 (2017).

[22] G. Falkovich and L. Levitov, Linking Spatial Distributions of Potential and Current in Viscous Electronics, Phys. Rev. Lett. **119**, 066601 (2017).

[23] A. D. Levin, G. M. Gusev, E. V. Levinson, Z. D. Kvon, and A. K. Bakarov, Vorticity-induced negative nonlocal resistance in a viscous two-dimensional electron system, Phys. Rev. B **97**, 245308 (2018).

[24] P. S. Alekseev and M. A. Semina, Ballistic flow of two-dimensional interacting electrons, Phys. Rev. B **98**, 165412 (2018).

[25] M. Chandra, G. Kataria, D. Sahdev, and R. Sundararaman, Hydrodynamic and ballistic AC transport in two-dimensional Fermi liquids, Phys. Rev. B **99**, 165409 (2019).

[26] J. A. Sulpizio, L. Ella, A. Rozen, J. Birkbeck, D. J. Perello, D. Dutta, M. Ben-Shalom, T. Taniguchi, K. Watanabe, T. Holder, *et al.*, Visualizing Poiseuille flow of hydrodynamic electrons, Nature (London) **576**, 75 (2019).

[27] T. Holder, R. Queiroz, T. Scaffidi, N. Silberstein, A. Rozen, J. A. Sulpizio, L. Ella, S. Ilani, and A. Stern, Ballistic and hydrodynamic magnetotransport in narrow channels, Phys. Rev. B **100**, 245305 (2019).

[28] M. Shavit, A. Shytov, and G. Falkovich, Freely Flowing Currents and Electric Field Expulsion in Viscous Electronics, Phys. Rev. Lett. **123**, 026801 (2019).

[29] O. E. Raichev, G. M. Gusev, A. D. Levin, and A. K. Bakarov, Manifestations of classical size effect and electronic viscosity in the magnetoresistance of narrow two-dimensional conductors: Theory and experiment, Phys. Rev. B **101**, 235314 (2020).

[30] A. Gupta, J. J. Heremans, G. Kataria, M. Chandra, S. Fallahi, G. C. Gardner, and M. J. Manfra, Hydrodynamic and Ballistic Transport over Large Length Scales in GaAs/AlGaAs, Phys. Rev. Lett. **126**, 076803 (2021).

[31] H. Guo, E. Ilseven, G. Falkovich, and L. S. Levitov, Higher-than-ballistic conduction of viscous electron flows, Proc. Natl. Acad. Sci. USA **114**, 3068 (2017).

[32] R. K. Kumar, D. A. Bandurin, F. M. D. Pellegrino, Y. Cao, A. Principi, H. Guo, G. H. Auton, M. Ben Shalom, L. A. Ponomarenko, G. Falkovich *et al.*, Superballistic flow of viscous electron fluid through graphene constrictions, Nat. Phys. **13**, 1182 (2017).

[33] L. V. Ginzburg, C. Gold, M. P. Röösli, C. Reichl, M. Berl, W. Wegscheider, T. Ihn, and K. Ensslin, Superballistic electron flow through a point contact in a Ga[Al]As heterostructure, Phys. Rev. Research **3**, 023033 (2021).

[34] A. Stern, T. Scaffidi, O. Reuven, C. Kumar, J. Birkbeck, and S. Ilani, Spread and erase - How electron hydrodynamics can eliminate the Landauer-Sharvin resistance, arXiv:2110.15369.

[35] C. Kumar, J. Birkbeck, J. A. Sulpizio, D. J. Perello, T. Taniguchi, K. Watanabe, O. Reuven, T. Scaffidi, A. Stern, A. K. Geim, and S. Ilani, Imaging hydrodynamic electrons flowing without Landauer-Sharvin resistance, arXiv:2111.06412.

[36] Yu. V. Sharvin, A possible method for studying Fermi surfaces, Sov. Phys. JETP **21**, 655 (1965).

[37] N. B. Abdallah, A hybrid kinetic-quantum model for stationary electron transport, J. Stat. Phys. **90**, 627 (1998).

[38] Y. Guo, Decay and continuity of the Boltzmann equation in bounded domains, Arch. Ration. Mech. Anal. **197**, 713 (2010).

[39] A. O. Govorov and J. J. Heremans, Hydrodynamic Effects in Interacting Fermi Electron Jets, Phys. Rev. Lett. **92**, 026803 (2004).

[40] R. N. Gurzhi, A. N. Kalinenko, and A. I. Kopeliovich, Electron-Electron Collisions and a New Hydrodynamic Effect in Two-Dimensional Electron Gas, Phys. Rev. Lett. **74**, 3872 (1995).

[41] R. N. Gurzhi, A. N. Kalinenko, and A. I. Kopeliovich, The theory of kinetic effects in two-dimensional degenerate gas of colliding electrons, Low Temp. Phys. **23**, 44 (1997).

[42] P. J. Ledwith, H. Guo, and L. Levitov, The hierarchy of excitation lifetimes in two-dimensional Fermi gases, Ann. Phys. **411**, 167913 (2019).

[43] P. Ledwith, H. Guo, A. Shytov, and L. Levitov, Tomographic Dynamics and Scale-Dependent Viscosity in 2D Electron Systems, Phys. Rev. Lett. **123**, 116601 (2019).

[44] O. E. Raichev, Linking boundary conditions for kinetic and hydrodynamic description of fermion gas, Phys. Rev. B **105**, L041301 (2022).

[45] H. H. Jensen, H. Smith, P. Wolfle, K. Nagai and T. M. Bisgaard, Boundary effects in fluid flow. Application to quantum liquids, J. Low Temp. Phys. **41**, 473 (1980).

[46] E. I. Kiselev and J. Schmalian, Boundary conditions of viscous electron flow, Phys. Rev. B **99**, 035430 (2019).